Alternating Conjugated and Nonconjugated Polymer. 1. Crystal Structures and Polymorphism of Poly(hexamethylene 2,2′-bithiophene-5,5′-dicarboxylate), P6BT

Shanger Wang and François Brisse*

Département de Chimie, Université de Montréal, C.P. 6128, Succursale A, Montréal, Québec, Canada H3C 3J7

Received November 26, 1997; Revised Manuscript Received January 22, 1998

ABSTRACT: X-ray fiber diffraction and DSC investigations of the title polymer, P6BT, reveal the existence of three polymorphs. Both α- and β-forms belong to the monoclinic system, while in the γ-form, the chains are packed in a triclinic unit cell. In all three forms the bithiophenedicarboxylate group is confined in a π-conjugated plane; however, with different orientations of the carbonyl group relative to the sulfur atom (in α- and β-froms, S−C−C═O is in the cis conformation, while in the γ-form, S−C−C═O is trans). The methylenic sequence in the β- and γ-forms is in the *all-trans* conformation with only slight deviations from planarity. With a torsion (τ_3) around the C−O bond between the aromatic plane and aliphatic segment, the polymer chain changes its overall shape from ribbonlike in the α-form ($\tau_3 \approx 180°$) to a sine-curve shape in the β-form ($\tau_3 = 173°$) and finally to a zigzag in the γ-form ($\tau_3 = 103°$). The α-form is paracrystalline, with random displacements of the chains along the fiber axis. The four chains in the unit cell of the β-form are found in two pairs displaced by 5.63 Å from each other, in the *c*-axis direction. Within the pair, the chains adopt an antiparallel disposition. The aromatic planes are arranged nearly parallel to the *ac* plane in a "side-by-side" pattern in the *a*-direction. Chains in the γ-form pack in successive layers, where the bithiophene dicarboxylic planes aggregate in a "face-to-face" fashion, forming well-organized π-stacks favorable for the interchain charge transfer of the alternating conjugated and nonconjugated polymer. The interplanar distance between neighboring bithiophene planes is 3.56 Å. The chain conformation and crystal packing in the γ-form resemble those observed in the model compound, di-*n*-hexyl 2,2′-bithiophene-5,5′-dicarboxylate (6BT6). A monotropic mesophase with unique chain arrangements was found to occur during heating. The transformation temperatures are as follows: α- to β-form, 130−150 °C; β- to γ-form, 161 °C; γ-form to mesophase, 172 °C; and mesophase to isotropic liquid, around 185 °C. The strong $\pi-\pi$ interaction between aromatic planes is believed to be the main driving force of the phase transformations. Due to this solid-state ordering process, the bathochromic shift in the UV−visible region was observed. Some abnormal phenomena such as preferred tilt of crystal in the γ-form are described. The relationship between these structures and those of the biphenyl analogue, poly(hexamethylene 4,4′-biphenyldicarboxylate) are discussed.

Introduction

The discovery of conducting polymers such as polyacetylene, polypyrrole, polythiophene, and polyaniline has led to numerous studies in the field of polymer science. Polythiophene is among the most extensively studied materials because it is a good conducting polymer with good environmental stability in both the neutral and doped forms.[1] Structure determination is an important goal for a better understanding of structure−property relationships of these conducting materials.[2−4] However, there is little structural information available from these conjugated polymers due to the difficulty in obtaining well-crystallized and fully oriented samples suitable for an X-ray structure analysis. Therefore, oligothiophenes have been widely investigated as structural models of the parent polymers.[5,6] However, they are independent small molecules and behave differently from the parent polymers in both crystallization process and structural organization. Incorporating the oligothiophenes into the polymer chain would impart them the characteristics of a macromolecule. The study of polymers with mixed conjugated and nonconjugated segments in the backbone chain will bridge the understanding between conducting polymers and small molecular crystals.[7,8]

Moreover, recent investigations on these polymers with well-defined oligomers indicated that they combine good mechanical properties and ease of processing with tunable electrical, electrochemical, and optical properties of conjugated polymers.[7−9] It was observed that polyesters derived from oligothiophenes exhibit efficient photophysical properties for preparing light-emitting diodes and a reversible redox process which may lead to the development of a novel electrochemical recording technique.[9] These studies demonstrated that intermolecular charge transport (hopping) through π-stacking plays an important role on electrochemical and photophysical properties. Structural studies of these alternating conjugated and nonconjugated polymers may provide valuable information about packing and conformational details of the conjugated parts of the polymer chain and the effects of the insulating segments. For this purpose, we have synthesized a series of polyesters composed of oligothiophene with different conjugated lengths and flexible, nonconjugated aliphatic segments. The polyesters schematically shown here were synthesized when $x = 2$ to 5 and $y = 5$ to 10. This

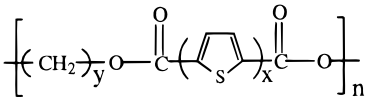

chemical structure was chosen mainly for the following two reasons: (1) The crystalline structures of the

S0024-9297(97)01735-X CCC: $15.00
Published on Web 03/10/1998

Scheme 1

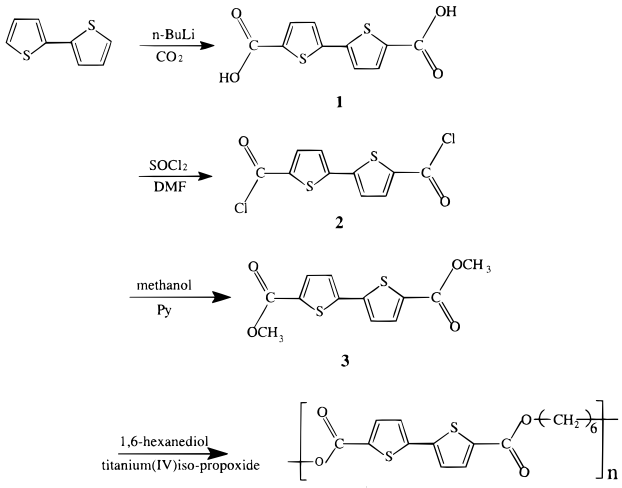

biphenylene analogues such as poly(ethylene 4,4′-biphenyldicarboxylate) and poly(hexamethylene 4,4′-biphenyldicarboxylate) have been established.[10,11] The structural information from these biphenylene analogues could be helpful in the structure determination of this new series of polyesters. (2) The polymers are potentially liquid crystalline, a useful property for obtaining higher electrical conductivity and anisotropic conductivity by virtue of spontaneous orientation of mesogens and macroscopic orientation of domain under an external forces such as shear stress and magnetic field.[12,13]

Experimental Section

Synthesis of Polymer P6BT and Model Compound 6BT6. At −78 °C, 5.6 mL of *n*-BuLi (2.5M) was added dropwise to a solution of 1.164 g (7 mmol) of 2,2′-bithiophene in 125 mL of THF. The mixture was allowed to warm to 0 °C for 30 min. It was then cooled back to −78 °C and treated with an excess of dry CO_2, which was generated by warming dry ice at 0 °C. The CO_2 was passed through a drying tube and concentrated H_2SO_4 and was bubbled through the mixture for 30min at −78 °C and then for 1h at room temperature before 3% KOH was introduced. The aqueous layer was washed 3 times with diethyl ether. The diacid **1** (Scheme 1) was precipitated by neutralizing the aqueous phase with 10% HCl. It was then collected by filtration, washed with water and dried. The diacid chloride **2** was obtained by refluxing the mixture of diacid and an excess of thionyl chloride in the presence of DMF for 24 h. The crude product was purified by recrystallization in CH_2Cl_2, yielding greenish needlelike crystals. Compound **2** was then esterified with methanol by refluxing for 24 h. The pure diester crystals, **3**, were obtained after recrystallizing them twice in DMF (yield 83%; mp 219.9 °C, by DSC). Following the same procedure, model compound, 6BT6, was synthesized using 1-hexanol (yield 75%, mp 71.0 °C, by DSC). Polarized microscopy examination and DSC measurements did not reveal the existence of a liquid crystalline phase.

The polymer was synthesized in a tube reactor charged with diester **3**, an excess of hexamethylene glycol, and a small amount of titanium(IV) isopropoxide. The mixture was stirred under N_2 at 225 °C when the reaction began. After 3 h, the temperature was progressively raised to 280 °C when the content became viscous. Finally, a vacuum of about 1 mmHg was applied in order to remove the excess diol. The resulting polymer was light yellow, flexible, and suitable for drawing fibers (T_g = 65 °C). The yield was 88%. The polymer is essentially insoluble in common organic solvents. NMR (300 MHz, CF_3COOD, ^1H, ppm): δ 7.75 (d, 2H), 7.25 (d, 2H), 4.40 (t, 4H), 1.85 (m, 4H), 1.55 (m, 4H). NMR (300 MHz, ^{13}C solid, ppm): δ 162.20 (s, 2C), 142.50 (s,2C), 135.10 (s, 4C), 126.15 (s, 2C), 68.00 (s, 2C), 31.35 (s, 2C), 29.70 (s, 2C).

Microscopic Observations. The liquid crystalline texture of P6BT was observed using a Leitz microscope under crossed polarizers. The temperatures were carefully calibrated using standard compounds with known T_m. The birefringent liquid crystalline phase with focal-conic texture was recorded when the polymer was heated above 172 °C. This mesophase was stable until the temperature was raised to 185 °C when it became a clear isotropic liquid.

Viscosity and Density Measurements. A 5 g/L solution of the polymer was prepared in a 60/40 (w/w) mixture of phenol and tetrachloroethane. The inherent viscosity, η_{inh}, determined at 25 °C with an Ubbelohde capillary viscosimeter was 1.12dL/g, indicating a polymer with a satisfactorily high molecular weight. The densities of the amorphous sample and fiber samples of the pure α- and γ-forms were measured by flotation in a $ZnCl_2$ aqueous solution. Three measurements were averaged, giving the values ρ_{amor} = 1.274 g·cm^{-3}, ρ_α = 1.309 g·cm^{-3}, and ρ_γ = 1.371 g·cm^{-3}. Since the β-form always coexists with the γ-form, the density data are not available.

Differential Scanning Calorimetry. DSC measurements were performed using a DuPont DSC 2100 apparatus. The scanning rate was 10 °C/min for the powder samples and 2.5 °C/min for the crystalline fibers in order to follow the crystal transformation process.

Infrared Spectroscopy. Photoacoustic FTIR spectroscopy was used in order to avoid damaging the sample or modifying the structure during the preparation of KBr pellets for conventional IR measurements.[14] Spectra of the P6BT fiber with different crystalline phase were taken on a Mattson Research Series FTIR spectrometer using an MTEC Model 300 photoacoustic cell. Fiber samples were simply cut into pieces (5−7 mm long) and placed into a sample cup. Samples were evaluated at a mirror speed of 0.98 cm/s (1.6 kHz) and a resolution of 8 cm^{-1}. The spectra were ratioed against the reference carbon black spectrum obtained from MTEC photoacoustics.[15]

Structure Determination of the Model Compound. Suitable single crystals of model compound, 6BT6, were obtained by slow evaporation from a methanol/petroleum ether mixture. X-ray intensity data collection was performed on an Enraf-Nonius CAD-4 automatic diffractometer, using the $\omega/2\theta$ scan technique and the monochromatized CuKα radiation (λ = 1.540 56 Å). The unit-cell dimensions (see Table 1) and orientation matrix were computed by a least-squares refinement of the angular settings of 25 well-centered reflections in the range 40° ≤ 2θ ≤ 50°. The stability of the crystal was monitored using five standard reflections whose intensites were measured every hour, and the orientation was checked every 100 reflections. The maximum fluctuation of the intensities of the reference reflections was 1.6%. After the data were reduced to a unique set of measurements, the diffracted intensities were corrected for Lorentz and polarization effects and an absorption correction based on the geometry of the crystal was applied.

The crystal structure of 6BT6 was solved by direct methods, using SHELXS96[16] and NRCVAX,[17] and finally refined by full-matrix least-squares methods.[18] The coordinates of the nonhydrogen atoms of 6BT6 were refined with anisotropic temperature factors. Hydrogen atoms were constrained to the parent sites using a riding model and refined isotropically. All the nonhydrogen atoms in the asymmetric unit were revealed in a difference Fourier synthesis. The midpoint of the central bond coincides with the crystallographic center of symmetry at (0,0,0). The refinements were weighted and based on F^2. The weighted R factor, R_w, and the goodness of fit, S, are based on F^2, while the conventional R factor, R, is based on F. Atomic scattering factors were taken from the ref 19. A summary of data collection and structure refinement is outlined in Table 1.

X-ray Diffraction of the P6BT Polyester. Amorphous filaments were drawn and quenched from the isotropic melt at 250 °C. Then they were stretched at room temperature into thin fibers with an average diameter of 0.1 mm. The fibers

Table 1. Crystal Data, Data Collection, and Structure Refinement for 6BT6

crystal data		data collection and structure refinement	
chem formula	$C_{11}H_{15}O_2S$	λ(Cu Kα), Å	1.54056
fw	211.29	$2\theta_{max}$, deg	140
unit cell	triclinic	T, K	293
space group	$P\bar{1}$	h, k, l ranges	$-5 \le h \le 5$
a, Å	4.768(1)		$-6 \le k \le 6$
b, Å	5.510(2)		$-28 \le l \le 28$
c, Å	23.298(13)	abs cor	integration
α, deg	91.29(4)	no. of measd reflcns	4308
β, deg	95.04(3)	no. of obsd reflcns, [$I > 2\sigma(I)$]	1281
γ, deg	106.78(3)	$R = \sum\|\|F_o\| - \|F_c\|\|/\sum\|F_o\|$, [$F^2 > 2\sigma(F^2)$]	0.056
V, Å^3	583.0(4)	$R_w = \{\sum[w(F_o^2 - F_c^2)^2]/\sum[w(F_o^2)^2]\}^{1/2}$	0.133
Z	2	$w = 1/[\sigma^2(F_o^2) + (0.072p)^2]$, $P = (F_o^2 + 2F_c^2)/3$	
F(000)	226	$S = \{\sum[w(F_o^2 - F_c^2)^2]/(n - p)\}^{1/2}$	1.089
d_o, g·cm^{-3}	1.19	(displacement)/$\sigma)_{max}$	0.025
d_c, g·cm^{-3}	1.204	(displacement)/$\sigma)_{mean}$	0.004
μ for Cu Kα, mm^{-1}	2.256	extreme values of residual electron density, e Å^{-3}	−0.22, 0.25
cryst size, mm	0.03 × 0.49 × 0.55		
cryst color	colorless		

were subjected to different annealing conditions before the diffraction patterns were recorded with a Philips X-ray generator using nickel-filtered Cu Kα radiation and a flat film Warhus camera. The sample-to-film distance was calibrated using NaF powder.

Structure Determination of P6BT. The indexing of the fiber patterns follows the description given in ref 11. The final values of the agreement index for the unit-cell dimensions refinement, R_c, expressed as $R_c = [\sum(\sin^2_{obs}\theta - \sin^2_{cal}\theta)^2/(n - 1)]^{1/2}$, were 0.038, 0.014, and 0.011 for the α-, β-, and γ-forms, respectively. The intensities of the reflection spots were visually estimated on a relative scale of 0−100. The intensity evaluation was carried out by 10 observers. Their results, which were in very good agreement, were then averaged.

The initial model of the structure was built using the geometrical data taken from the model compound and from other related compounds whose structures were taken from the Cambridge Structure Database (CSD).[20] Before energy minimization, some torsion angles were modified so that the chain had a fiber repeat equivalent to the experimental value. The chain was then translated and rotated within the unit cell so that the simulated fiber pattern approaches that of the experimental one. Different symmetry constraints were applied in case of multiple choice of space group, and the structure factors were calculated after Lorentz and polarization corrections were applied. The chain and then the total packing potential energy of the structure were minimized using the Cerius2 release 2.0 package[21] running on a Silicon Graphics IRIS work station with an Indigo processor. The Dreiding force field[22] and Polak-Ribiere conjugate-gradient technique were employed. During the energy minimization, the cell parameters were kept constant and the bithiophene moiety was set as a rigid unit at the beginning and subjected to minor changes before the final model was reached.

Results and Discussion

Structure of the Model Compound. A perspective representation of the 6BT6 molecule and the atomic numbering are shown in Figure 1a. It is of interest to note that the two units which make up the molecule, the bithiophene moiety and the aliphatic sequence, are both ordered. The molecule, which is centrosymmetric, consists of a planar bithiophene group (rms deviation = 0.006 Å) with the sulfur atoms in trans to one another. The methylenic sequence of atoms is essentially all-trans since the largest deviation from 180° is 10°. These two units are connected by an ester group which is nearly coplanar with the adjacent thiophene ring (dihedral angle 1.6°, Table 2). The carbonyl group is trans relative to the sulfur atom of the adjacent thiophene. This disposition is the most frequently observed in

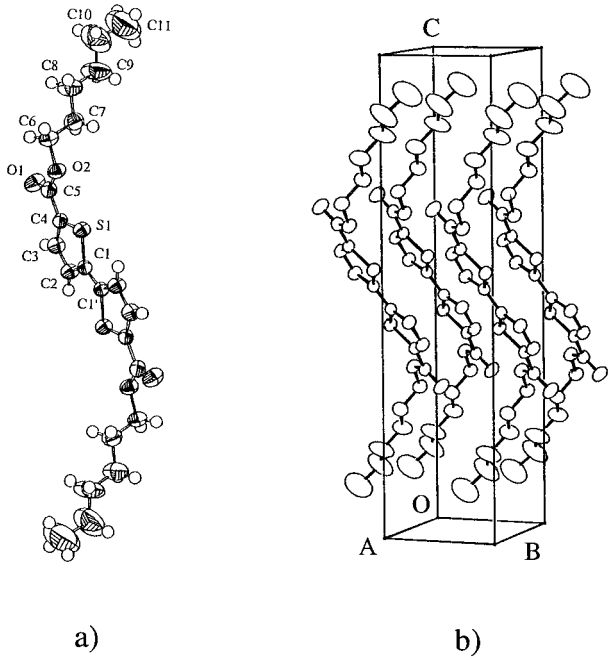

Figure 1. Atomic numbering and molecular packing of 6BT6.

thienylcarboxylates.[23] The shape of the 6BT6 molecule can be best described as that of the letter "Z", with the sharp turn located at the torsion of C5−O−C6−C7 (90.1°). It can be seen that, in this orientation, as Figure 1b shows, the aromatic groups in different molecules are closely arranged in a "face-to-face" pattern, forming π-stacks which favor the lowest energy of the system. The interplanar distance between the conjugated thiophene planes is 3.53 Å. This value is comparable to that observed in α,α'-dimethylquaterthiophene (3.50 Å),[24] α-sexithiophene (3.56 Å),[25] and α-octithiophene (3.53 Å).[26] The length of the central C−C′ bond is 1.433(6) Å, which is a little shorter than the corresponding distance in 2,2′-bithiophene (1.448(4) Å).[27] This shortening is possibly due to the electron-accepting effect of the carbonyl substituent. The fractional atomic coordinates and equivalent isotropic displacement parameters, U_{eq}, are presented in Table 3. The relatively larger U_{eq} values observed for the last three methylenic carbons may be due to their enhanced thermal vibration.

Identification of the Polymorphs and Determination of the Lattice Parameters. A unique X-ray

Table 2. Selected Geometrical Parameters in the Bithiophene Moiety and the Aliphatic Segment of 6BT6

bond distance (Å)		bond angle (deg)	
S1−C4	1.709(3)	S1−C1−C2	109.7(2)
S1−C1	1.723(3)	C1−C2−C3	113.9(3)
C1−C2	1.362(4)	C2−C3−C4	113.0(3)
C2−C3	1.394(5)	C3−C4−S1	111.0(3)
C3−C4	1.356(4)	C4−S1−C1	92.4(2)
C1−C1′	1.433(6)	S1−C1−C1′	120.9(3)
O1−C5	1.188(4)	C2−C1−C1′	129.4(4)
O2−C5	1.346(4)	C5−C4−S1	122.6(2)
O2−C6	1.452(4)	O2−C5−C4	110.7(3)
C4−C5	1.469(5)	O1−C5−O2	124.2(3)
C6−C7	1.488(5)	C5−O2−C6	117.3(3)
C7−C8	1.479(5)	O2−C6−C7	110.7(3)
C8−C9	1.499(7)	C6−C7−C8	114.3(4)
C9−C10	1.422(8)	C7−C8−C9	113.1(5)
C10−C11	1.479(10)	C8−C9−C10	114.9(6)
		C9−C10−C11	110.3(9)

torsion angle (deg)		dihedral angle (deg)	
C1−S1−C4−C5	179.9(3)	$\Psi_{\text{thiophene−thiophene}}$	0.00
S1−C4−C5−O1	−178.2(3)	$\Psi_{\text{thiophene−ester group(C(=O)−O)}}$	1.61
C4−C5−O2−C6	−176.2(3)		
C5−O2−C6−C7	90.1(4)		
O2−C6−C7−C8	169.9(4)		
C6−C7−C8−C9	−176.9(5)		
C7−C8−C9−C10	170.2(8)		
C8−C9−C10−C11	−177.6(9)		

Table 3. Fractional Atomic Coordinates, Their Esd's, and Equivalent Isotropic Thermal Parameters (Å²) for 6BT6

atom	*x*	*y*	*z*	U_{eq}[a]
S1	0.6403(2)	0.8961(1)	0.4312(1)	0.0721(3)
O1	0.5030(5)	1.2888(5)	0.2997(1)	0.1015(9)
O2	0.2539(5)	0.9123(4)	0.3304(1)	0.0812(7)
C1	0.9540(6)	1.0552(6)	0.4747(1)	0.0610(8)
C2	1.0815(7)	1.2836(6)	0.4527(2)	0.0765(9)
C3	0.9312(7)	1.3297(6)	0.4020(1)	0.0780(10)
C4	0.6843(7)	1.1380(6)	0.3850(1)	0.0640(8)
C5	0.4781(7)	1.1284(7)	0.3337(2)	0.0731(9)
C6	0.0407(8)	0.8672(7)	0.2800(1)	0.0863(11)
C7	0.1304(9)	0.7264(9)	0.2331(2)	0.1064(13)
C8	−0.0981(11)	0.6332(11)	0.1841(2)	0.1390(19)
C9	−0.0080(15)	0.4801(16)	0.1390(2)	0.206(4)
C10	−0.237(2)	0.353(2)	0.0960(4)	0.278(5)
C11	−0.128(3)	0.199(2)	0.0554(4)	0.345(6)

[a] $U_{eq} = (1/3)\sum_i\sum_j U_{ij} a_i^* a_j^* \mathbf{a}_i.\mathbf{a}_j$.

diffraction pattern of P6BT was obtained by annealing the stretched fiber at 120 °C. It is shown in Figure 2a. The characteristic feature of this pattern is the presence of two outstandingly strong reflections on the equator and continuous streaks on all layer lines. The fiber repeat was found to be 19.61 Å, indicating that in the α-form the chain is essentially in the fully extended conformation with the carbonyl group cis relative to the sulfur atom in the adjacent thiophene (see the following discussion). Indexing of the fiber pattern yielded a monoclinic unit cell having dimensions of $a = 11.88$ Å, $b = 10.77$ Å, $c = 19.61$ Å, and $\beta = 91.8°$. Six polymer chains must pass through the unit cell to have the calculated density (1.337 g/cm^3) close to the observed value (1.309 g/cm^3). The calculated and observed *d*-spacings are compared in Table 4. Since the reflections on the layer lines are not well resolved and a few reflections are superimposed as shown in Table 4, neither the chain conformation nor the space group could be established. It is suggested that the α-form is in a paracrystalline state,[28] where the polymer chains themselves have a longitudinal periodic conformation and have positional order in the lateral direction, while the arrangement of the chains along the fiber direction is random. Because of the paracrystalline nature, the melting point of the α-form largely depends on the annealing temperature, i.e., shifting progressively to higher temperatures upon increasing of the annealing temperature (Figure 3). When the annealing temperature is above 150 °C, the reflections of the α-form disappear gradually, and a new diffraction pattern is observed (Figure 2c). This fiber pattern is composed of more than one crystalline form, and no reasonable unit cell, taking into account all the diffraction spots, could be deduced. By annealing this fiber at about 170 °C for 2 days, some of the diffraction spots completely disappear and a clear well-resolved diffraction pattern emerges (Figure 2b). All the reflections correspond to a single crystalline phase, which is called the γ-form. The lattice parameters are $a = 5.54$ Å, $b = 4.71$ Å, $c = 17.90$ Å, $\alpha = 113.7°$, $\beta = 96.7°$, and $\gamma = 106.6°$. Since the observed density is 1.371 g/cm^3, only one chain passes through the unit cell, leading to a calculated density of 1.414 g/cm^3. The observed and calculated *d*-spacings, compared in Table 5, are in a very good agreement. It is worth indicating that the diffraction spots in Figure 2b are not perfectly aligned on their respective layer lines. Thus, the chain axis is tilted, by a few degree, from the fiber axis. This behavior is quite comparable to the well-characterized situation described for poly(alkylene terephthalates)[29] and P6BP.[11] On the basis of the geometric relationship, the reciprocal space coordinates (ξ, ζ) can be calculated from the film coordinates.[11] The good agreement between the calculated and observed ζ values, the distance from reciprocal lattice point to equatorial plane, provided a powerful confirmation of the correctness of the indexing. Thus, the tilt angle, μ, can be deduced from the angles of the reciprocal axis relative to the fiber orientation ($\phi_a = 92.4°$, $\phi_b = 94.1°$, $\phi_c = 31.9°$). The tilt angle μ, which is the difference between ϕ_c and ϕ_{nt} (angle between c^* and the fiber axis without tilting) has a value of 5.2°. The origin of the preferred tilt although not very clear, must be associated with the crystallization mechanism or, in this case, the crystalline phase transformation. On one hand, the crystalline motives have a tendency to self-organize in their allowed free volume and form a three-dimensionally ordered structure by overcoming the activation energy of crystallization; on the other hand, the motion of the chain segments is hindered by the macroscopic high viscosity of the system and the microscopic interchain and intrachain interactions. In the fiber samples, the stress imposed on the molecular chains is highly anisotropic, and the stress component along the fiber axis is relatively larger than the others. Therefore, it can be envisaged that, during crystallization, the motion of the crystalline motif is also anisotropic and behaves in such a way that the minimum energy gap is overcome in order to meet the crystallographic requirements, and in this particular case, the preferred tilt is adopted. It is notable that, among the three crystalline forms of P6BT, the phenomenon is observed only in the high temperature γ-form. As will be illustrated in the following discussion, the repeat unit of the γ-form is significantly shorter than those in the α- and β-forms. This means that the chains are subjected to a shrinking deformation, which is severely restricted by longitudinal stress. Therefore, the chain segments, which have presumably the dimension of crystalline lamellar thickness, prefer to tilt by a few

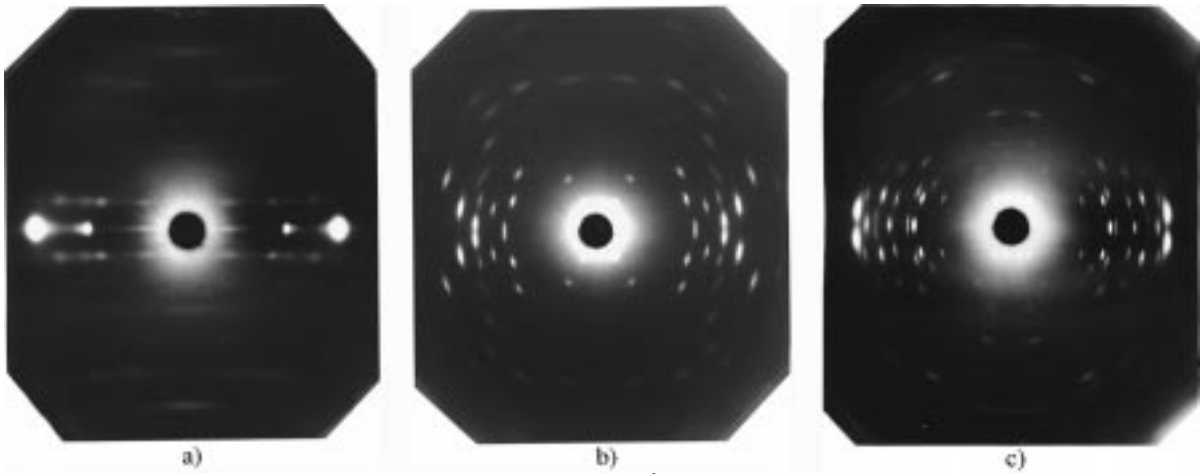

Figure 2. X-ray fiber patterns of P6BT: (a) α-form; (b) γ-form; (c) β-form (which includes a small proportion of the γ-form).

Table 4. Comparison of the Calculated and Observed *d*-Spacings and Estimated Intensities for the α-Form

spot no.	*h k l*	d_{cal}, Å	d_{obs}, Å	intensity[a]
1	1 0 0	11.874	11.99	w
2	0 2 0	5.385	5.28	vs
	2 1 0	5.199		
3	1 2 0	4.904	4.83	w
4	3 0 0	3.958	3.98	w
	2 2 0	3.989		
5	0 3 0	3.590	3.60	vs
	3 1 0	3.715		
6	1 0 −1	10.299	10.33	w
	1 0 1	10.018		
7	2 0 −1	5.732	5.81	s
8	2 2 −1	3.924	4.07	s
	3 0 −1	3.904		
9	2 3 −1	3.043	2.91	vw
	4 0 −1	2.949		
	4 0 1	2.922		
10	0 2 1	5.193	4.99	w
	2 1 −1	5.060		
	2 1 1	4.992		
11	3 1 1	3.631	3.66	vw
	0 3 1	3.531		
12	0 2 2	4.720	4.78	vw
	2 1 −2	4.646		
13	0 0 3	6.534	6.44	w
14	1 0 4	4.481	4.48	w
	0 1 4	4.460		
15	0 2 4	3.624	3.66	vw
	2 1 4	3.616		
16	1 0 5	3.688	3.60	w
	0 1 5	3.684		
17	2 0 5	3.225	3.26	w
	2 1 −5	3.172		
	0 2 5	3.169		
18	1 0 −6	3.175	3.14	s
	0 1 6	3.126		
	1 0 6	3.125		
19	3 0 −6	2.559	2.57	w
	2 2 −6	2.554		
20	0 1 7	2.710	2.66	w
	1 0 7	2.707		
	1 1 −7	2.660		
21	0 3 7	2.208	2.21	w
	3 1 7	2.205		

[a] Estimated intensity: vs, very strong; s, strong; w, weak; vw, very weak.

degrees around the center of the crystalline segments, rather than undergo a more difficult translation.

Extensive efforts have been made in order to obtain the fiber pattern of the pure β-form. However, a perceivable amount of the γ-form always exists. Nevertheless, the majority of the reflections belong to a different crystalline form, the β-form (Figure 2c). All 44 reflections can be indexed with a monoclinic cell of dimensions of $a = 11.22$ Å, $b = 7.87$ Å, $c = 38.60$ Å, and $\beta = 104.8°$. The calculated crystal density, 1.357 g/cm^3, indicates that there are four polymer chains in this unit cell. The observed and calculated *d*-spacings are compared in Table 6. The large number of reflections suggests that the β-form is in a well crystallized state, which has a relatively well-defined melting point (ca. 151 °C, Figure 3).

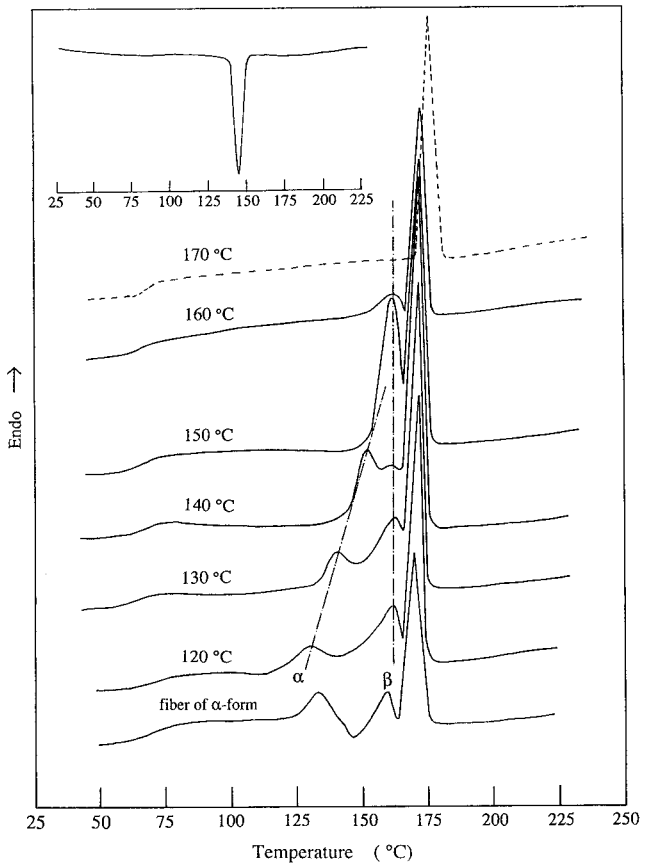

Figure 3. DSC heating scans (rate, 10 °C/min) of P6BT powder after 30 min annealing at different temperatures and of the pure α-form (2.5 °C/min). A cooling scan is also included in upper left.

In summary, when the P6BT raw fibers are annealed below 130 °C, only the paracrystalline α-form is developed. As the annealing temperature increases, the α-form is transformed into the β- and the γ-forms, whose

Table 5. Comparison of the Observed and Calculated *d*-Spacings, ζ Values and Structure Factors of the γ-form.

spot no.	*h k l*	d_{cal}, Å	d_{obs}, Å	ζ_{cal}, Å^{-1}	ζ_{obs}, Å^{-1}	$\|F_{cal}\|^a$	$\|F_{obs}\|$	*w*
1	1 0 0	5.119	5.11	0.0081	0.009	1.748	2.06	1
2	0 1 0	4.014	4.00	0.0177	0.017	4.280	4.43	1
3	1 1 0	2.713	2.72	0.0258	0.027	1.417	1.30	1
4	0 0 1	15.818	15.72	0.0537	0.054	1.789	2.01	0.7
5	1 0 1	4.533	4.54	0.0456	0.045	2.383	2.31	1
6	1 0 −1	5.295	5.30	0.0617	0.062	2.222	2.65	1
7	1 −1 1	4.057	4.07	0.0633	0.062	2.123	1.90	1
8	−1 1 1	3.615	3.61	0.0440	0.044	4.765	5.01	1
	0 1 1	3.526		0.0360				
9	1 1 −1	2.899	2.90	0.0796	0.080	1.558	1.78	1
10	2 0 −1	2.638	2.64	0.0697	0.069	1.191	1.19	0.5
11	0 0 2	7.909	7.87	0.1073	0.110	0.808	0.89	0.7
12	1 0 −2	4.929	4.93	0.1154	0.116	2.397	2.01	1
13	1 0 2	3.859	3.87	0.0992	0.097	1.637	1.69	1
14	0 1 −2	4.504	4.50	0.1250	0.123	0.532	0.42	0.5
15	−1 1 2	3.221	3.22	0.0976	0.097	4.157	3.75	1
16	1 −1 2	3.926	3.93	0.1170	0.118	1.286	1.29	1
17	0 1 −3	4.268	4.27	0.1786	0.178	0.810	0.55	0.5
18	1 −1 3	3.605	3.60	0.1706	0.171	2.010	1.61	1
19	0 0 4	3.954	3.93	0.2146	0.216	0.408	0.46	0.5
20	1 0 −4	3.625	3.63	0.2227	0.224	0.748	0.73	0.5
21	1 −1 4	3.210	3.21	0.2242	0.224	1.827	1.45	1
22	1 1 −4	2.933	2.93	0.2404	0.244	1.394	1.11	1
23	1 0 4	2.794	2.80	0.2061	0.198	0.718	0.86	0.7
24	−1 1 4	2.499	2.50	0.2050	0.207	0.795	0.92	0.7
25	0 0 5	3.164	3.17	0.2683	0.269	1.848	1.55	0.7
26	1 0 5	2.421	2.42	0.2602	0.261	0.820	0.85	0.7
27	0 1 −5	3.332	3.34	0.2859	0.286	0.652	0.82	0.7
28	0 0 6	2.636	2.65	0.3219	0.325	0.959	0.98	1
	1 0 −6	2.644		0.3299				0.5
29	1 1 −6	2.545	2.55	0.3476	0.350	1.293	1.20	0.7

[a] For overlapped spots, $F_{cal} = (\Sigma F_{cal.ref}{}^2)^{1/2}$.

Table 6. Comparison of the Observed and Calculacted *d*-Spacings and Structure Factors of the β-Form

spot no.	*h k l*	d_{cal}, Å	d_{obs}, Å	$\|F_{cal}\|$	$\|F_{obs}\|^a$	*w*
1	2 0 0	5.426	5.43	2.787	3.09	1
2	4 0 0	2.712	2.71	0.603	0.40	0.5
3	2 1 0	4.466	4.41	1.340	2.02	1
4	0 2 0	3.935	3.78	3.603	3.22	1
5	1 1−1	6.442	6.26	1.208	1.11	0.5
	1 1 1	6.130				
6	3 1 1	3.209	3.19	1.337	1.44	0.5
7	1 2 1	3.650	3.58	8.070	8.09	1
	1 2 −1	3.713				
8	0 0 2	18.662	18.37	1.335	1.44	0.7
9	2 0 −2	5.606	5.61	3.664	3.76	1
10	2 0 2	4.886	4.89	0.562	0.40	0.5
11	4 0 −2	2.787	2.79	0.939	1.11	0.5
12	0 1 2	7.252	7.05	0.926	1.32	0.5
13	2 1 −2	4.566	4.62	1.299	1.48	0.5
14	2 1 2	4.151	4.11	3.529	3.72	1
15	0 2 2	3.850	3.72	1.494	1.46	0.5
16	1 1 −3	6.050	5.93	2.102	1.53	0.7
17	1 1 3	5.354	5.36	1.471	0.86	0.5
18	3 1 −3	3.376	3.36	0.472	0.70	0.5
	1 2 3	3.464				
19	3 1 3	3.010	2.99	0.184	0.38	0.5
20	1 2 −3	3.633	3.51	0.867	0.80	0.5
21	2 0 −4	5.315	5.33	0.540	0.55	0.5
22	2 0 4	4.243	4.21	1.591	1.44	0.5
23	4 0 −4	2.803	2.80	1.064	0.96	0.5
24	0 1 4	6.016	5.88	0.262	0.26	0.5
25	2 1 −4	4.405	4.37	1.477	1.28	1
26	2 1 4	3.735	3.71	1.305	1.20	0.5
27	4 1 −4	2.641	2.64	0.751	0.70	0.5
28	0 0 6	6.221	6.20	0.636	0.71	1
29	0 0 8	4.666	4.63	1.073	1.17	1
30	2 0 8	3.161	3.20	0.645	0.52	0.5
31	4 0 −8	2.658	2.66	0.983	0.81	0.5
32	2 1 8	2.933	2.91	0.844	0.54	0.5
33	0 0 10	3.732	3.72	0.266	0.36	1
34	0 1 10	3.372	3.35	1.758	1.57	1
35	1 1 −11	3.200	3.17	0.668	0.72	1
36	0 0 12	3.110	3.10	1.497	1.65	1
37	2 0 12	2.443	2.43	1.911	1.91	0.7
38	0 1 12	2.893	2.88	0.944	1.33	0.5
39	1 1 −13	2.778	2.76	0.707	0.79	0.5
40	1 2 −13	2.370	2.34	1.324	1.53	0.5
41	0 0 14	2.666	2.70	0.288	0.47	0.7
42	4 0 −14	2.203	2.20	1.618	1.63	0.5
	2 0 14	2.183				
43	2 1 −14	2.535	2.52	0.245	0.64	0.5
44	4 1 −14	2.121	2.12	1.217	1.25	0.5
	2 1 14	2.103				

[a] For overlapped spots, $F_{cal} = (\Sigma F_{cal.ref}{}^2)^{1/2}$.

relative contents depend on the annealing conditions (time, temperature, and external stress). The X-ray diffraction patterns of more than 50 fibers which underwent various annealing treatments reveal that a moderate temperature and short annealing time favor the formation of the β-form, while prolonged annealing at higher temperature favors the growth of the γ-form. This result suggests that the α to β transformation is kinetically controlled, while the α to γ transformation is thermodynamically controlled. Structural differences may account for this assumption. As will be illustrated in the following discussion, the difference between the α- and the γ-forms is much more significant than that between the α- and the β-forms, in both the chain conformation and packing arrangement. Thus, the β-form can be attained by small adjustments of the chain's orientation and disposition, i.e., overcoming a low energy barrier. However, this form is also thermodynamically metastable and can, therefore, be transformed into the thermodynamically stable γ-form by further annealing at elevated temperature. The fiber of the pure γ-phase is readily attainable in this manner. The crystal data of interest of three polymorphs are collected in Table 10.

From DSC scans, one may get some insights into the crystalline transformation mechanism. On the DSC curve of the pure α-form of the P6BT fiber (the lowest curve in Figure 3), a melting endotherm of α-form immediately followed by a crystallization exotherm is observed in the 125−150 °C temperature range. This is the typical DSC behavior of the crystal melting and recrystallization process.[30] Considering that the chains have to perform a remarkable modification to accomplish the crystal transformation, the chains in the β-form have to be thawed first by melting to gain enough mobility in order to adjust their conformation and position. In this respect, the same melting and recrystallization mechanism is plausible for the β- to γ-crystal transformation, although no distinctive crystallization exotherm was observed following the melting of the β-crystals, which may due to the partial overlap of the melting endotherm and the following crystallization exotherm.[31]

Chain Structure and Crystal Packing. α-Form. Figure 4 depicts the fully extended conformation of P6BT and P6BP, and their calculated fiber repeats. The carbonyl group adjacent to the bithiophene may adopt two orientations (*cis* or *trans*) relative to the sulfur atom, giving rise to significantly different fiber repeat lengths of 19.66 and 17.88 Å. The observed fiber repeat of the α-form is 19.61 Å, a value nearly equal to that calculated for the fully extended repeat unit, when the S−C−C═O torsion angle is 0° (*cis* conformation). Obviously, the aliphatic sequence of P6BT is in the *all-trans* conformation (planar zigzag) with very little deviation

Table 7. Comparison of the Torsion and Dihedral Angles(deg) in 6BT6, β-P6BT and γ-P6BT

torsion angles		6BT6	γ-P6BT	β-P6BT
S1−C4−C5−O2	τ_1	2.2	0.3	−177.8
C4−C5−O2−C6	τ_2	−176.2	−177.4	178.7
C5−O2−C6−C7	τ_3	90.1	103.2	−172.8
O2−C6−C7−C8	τ_4	169.9	175.2	−178.4
C6−C7−C8−C8′	τ_5		176.8	−176.5
C7−C8−C8′−C7′	τ_6		180.0	179.4
C8−C8′−C7′−C6′	$\tau_{5'}$			171.4
C8′−C7′−C6′−O2′	$\tau_{4'}$			−175.6
C7′−C6′−O2′−C5′	$\tau_{3'}$			171.2
C6′−O2′−C5′−C4′	$\tau_{2'}$			178.6
O2′−C5−C4′−S1′	$\tau_{1'}$			180.0

dihedral angles [plane−plane]		6BT6	γ-P6BT	β-P6BT
[S1−C1−C2−C3−C4]−[S1′−C1′−C2′−C3′−C4′]	Φ	0.0	0.0	0.6
[S1−C1−C2−C3−C4]−[C5(═O1)−O2]	ϵ	0.7	1.7	2.1
[S1′−C1′−C2′−C3′−C4′]−[C5′(═O1′)−O2′]	ϵ′		−1.7	0.4

Table 8. Fractional Atomic Coordinates of the β-Form

	chain 1			chain 2		
atom	*x*	*y*	*z*	*x*	*y*	*z*
S1	0.0568	0.6207	−0.1240	0.1375	0.1386	0.0230
O1	−0.0531	0.6426	−0.2039	0.0299	0.1474	−0.0567
O2	0.1260	0.6747	−0.2201	0.2102	0.1428	−0.0731
C1	0.1998	0.6310	−0.0929	0.2801	0.1354	0.0542
C2	0.2955	0.6445	−0.1098	0.3772	0.1299	0.0377
C3	0.2551	0.6531	−0.1467	0.3377	0.1324	0.0007
C4	0.1273	0.6443	−0.1588	0.2090	0.1384	−0.0117
C5	0.0620	0.6532	−0.1949	0.1454	0.1432	−0.0479
C6	0.0780	0.6910	−0.2580	0.1623	0.1435	−0.1112
C7	0.1870	0.7336	−0.2742	0.2719	0.1712	−0.1280
C8	0.1485	0.7528	−0.3155	0.2330	0.1888	−0.1694
S1′	0.3504	0.8748	−0.5232	0.4333	0.3662	−0.3771
O1′	0.4587	0.8582	−0.4436	0.5435	0.3478	−0.2970
O2′	0.2791	0.8603	−0.4269	0.3644	0.3182	−0.2806
C1′	0.2076	0.8804	−0.5542	0.2899	0.3650	−0.4079
C2′	0.1108	0.8866	−0.5376	0.1942	0.3547	−0.3909
C3′	0.1506	0.8815	−0.5006	0.2351	0.3437	−0.3540
C4′	0.2784	0.8729	−0.4884	0.3631	0.3476	−0.3420
C5′	0.3432	0.8635	−0.4523	0.4283	0.3384	−0.3059
C6′	0.3283	0.8522	−0.3890	0.4121	0.3026	−0.2426
C7′	0.2187	0.8271	−0.3721	0.3039	0.2591	−0.2262
C8′	0.2582	0.8055	−0.3309	0.3420	0.2433	−0.1849

Table 9. Fractional Atomic Coordinates of the γ-form

atom	*x*	*y*	*z*
S1	−0.0106	−0.1540	0.1009
O1	0.5945	0.1531	0.2884
O2	0.1764	−0.1945	0.2583
C1	0.0934	0.0176	0.0352
C2	0.3583	0.2165	0.0660
C3	0.4770	0.2302	0.1404
C4	0.3032	0.0400	0.1677
C5	0.3678	0.0027	0.2402
C6	0.1955	−0.2592	0.3298
C7	0.0717	−0.0462	0.3915
C8	0.0561	−0.1134	0.4688
H2	0.4499	0.3293	0.0396
H3	0.6525	0.3534	0.1686
H6a	0.0887	−0.5235	0.3080
H6b	0.3979	−0.1990	0.3608
H7a	−0.1251	−0.0983	0.3574
H7b	0.1879	0.2163	0.4131
H8a	−0.0695	−0.3727	0.4470
H8b	0.2512	−0.0756	0.5009

from the 180° planar zigzag situation. As observed in many thienylcarboxylates, the carboxylic group is nearly coplanar with the adjacent ring and the torsion (S−C−C═O) is of either the *cis* or the *trans* conformation (Figure 5). Furthermore, the two carboxylic groups are in the *E*-conformation, the most frequently observed situation.

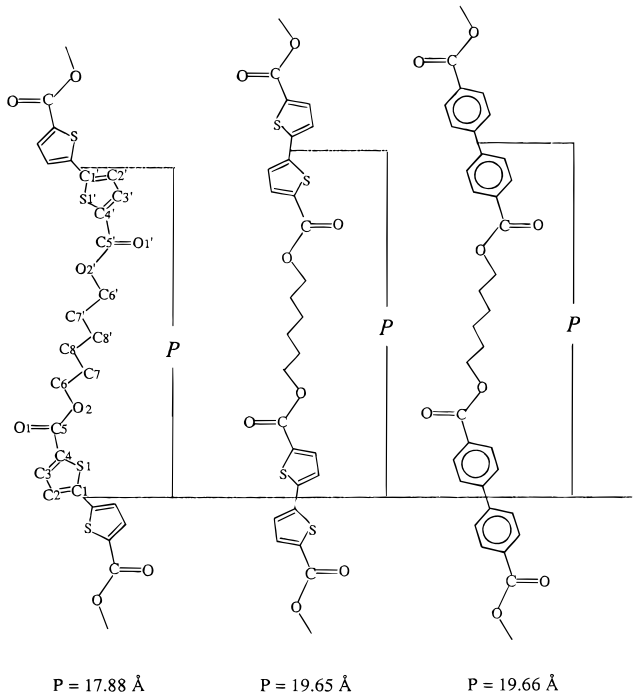

P = 17.88 Å P = 19.65 Å P = 19.66 Å

Figure 4. Comparison of fiber repeats for the fully extended conformation in P6BT and P6BP (in reference to Li et al.[11]).

Table 10. Crystal and Physical Data of the Three Forms of P6BT

parameter	α-P6BT	β-P6BT	γ-P6BT
monomer unit	$S_2C_{16}H_{16}O_4$	$S_2C_{16}H_{16}O_4$	$S_2C_{16}H_{16}O_4$
transition temp, °C	131−150	161	172
$T_{determine}$, K	298	298	298
unit cell	monoclinic	monoclinic	monoclinic
a, Å	11.88	11.22	5.54
b, Å	10.77	7.87	4.71
c, Å	19.61	38.60	17.90
α, deg	90	90	113.7
β, deg	91.8	104.8	96.7
γ, deg	90	90	106.6
V, Å^3	2507	3295	395
Z	6	8	1
d_o(amorphous), g·cm^{-3}	1.274	1.274	1.274
d_{obs}, g·cm^{-3}	1.309		1.371
d_{cal}, g·cm^{-3}	1.337	1.357	1.414
space group		$P2_1/c$	$P\bar{1}$
h, *k*, *l* ranges	$0 \le h \le 4$ $0 \le k \le 3$ $-6 \le l \le 7$	$0 \le h \le 4$ $0 \le k \le 2$ $-14 \le l \le 14$	$-2 \le h \le 2$ $-1 \le k \le 1$ $-6 \le l \le 6$
no. of unique diffraction spots	21	44	29
$R = \sum\|\Delta F\|/\sum\|F_o\|$		0.148	0.116
$R_w = [\sum w(\|F_o\| - \|F_c\|)^2/\sum wF_o^2]^{1/2}$		0.142	0.115
B_{iso}, Å^2		18.9	15.9
tot. packing energy, kcal/mol		−37.4	−39.7

Theoretical calculations[32,33] and X-ray crystal structure studies[24−27,34−39] so far proved that α,α′-oligothiophenes have most frequently a coplanar structure with an anti-arrangement between adjacent rings. It is suggested that by assuming this conformation, the system sustains the maximum $\pi-\pi$ conjugation. The same reason may account for the coplanarity between the thiophene and the carbonyl groups.

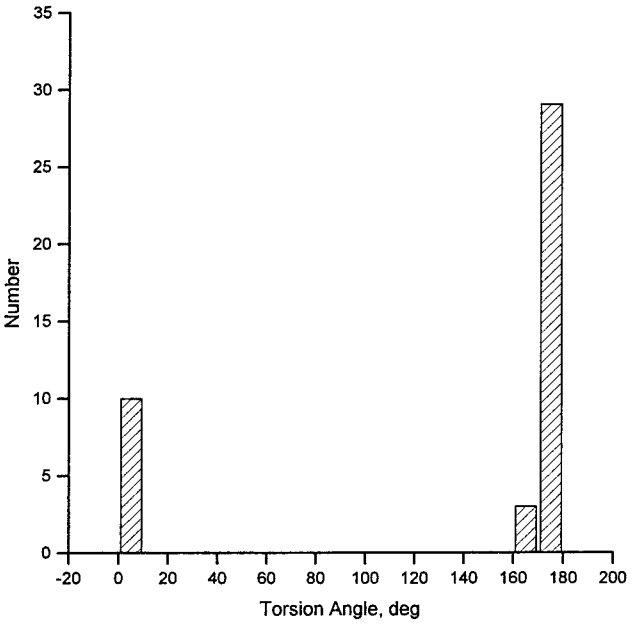

Figure 5. Distribution of the S−C−C═O torsion angle in thienylcarboxlates. Data are cited from the Cambridge Data Files with the following REFCODES: BCXDTH, CACTHP, DACLIC, DENHIN, FEGNAG, IPTHBZ, JERYUA, MTHPHE, MTHPHE01, SEBCOR, TPENAC, TPENAC01, TPENAC02, VANDIX, VEGNIE, VEGNOK, VIBRED, VORKOC, WEKZIV, WIFRIM, YAGDEP, YAGDIT, YAYBAB, ZEDQII, ZEJFUP, ZEJHIF, ZEWCEJ, and ZOTSIK.

As mentioned earlier, the α-form is of a paracrystalline nature, therefore, it is difficult to describe the details of the chain packing. However, some structural information can be deduced from its fiber pattern shown in Figure 2a. The strongest two reflections, having *d*-spacings of 3.60 and 5.28 Å (Table 4), are found on the equator. The former has almost three times the intensity of the latter. The very strong intensities and their ratio suggest that the flat ribbon-shaped molecules are placed in the cell in such a way as to contribute mainly, in terms of electronic density, to these two crystallographic planes. Then, by rotating the chains, we found a most likely herringbone type of packing projected onto the *ab* plane (Figure 6a), when the good agreement between observed and calculated intensities for the *hk*0 reflections is achieved (Figure 6b).

***β*-P6BT.** In the *β*-form, the fiber repeat ($p = 2 \times 19.30$ Å) is slightly shorter than twice the length of a monomer unit in a fully extended conformation. However, as can be seen in Table 7, the chain possesses, in the first approximation, the same features as the α-form. The bithiophenedicarboxylate moiety is essentially coplanar, and the two carboxylic groups are in the *E*-conformation. The aliphatic segment is also in the *all-trans* conformation. The molecular chain has the shape of a sine wave fluctuating up and down in the *b*-axis direction (Figure 7a). The four chains in the unit cell are grouped into two pairs. In each pair, the two chains adopt an anti-parallel disposition along the *c*-axis direction, and the thiophene planes, arranged in a side-by-side fashion in the *b*-axis direction, are roughly parallel to the *bc* plane. The two molecular pairs are displaced from each other by 5.63 Å along the *c*-axis. No $\pi-\pi$ interaction could be expected in this type of packing.

The condition on the indices of the 44 diffraction spots given in Table 6, i.e., for $h0l$, $l \neq 2n$, indicates the

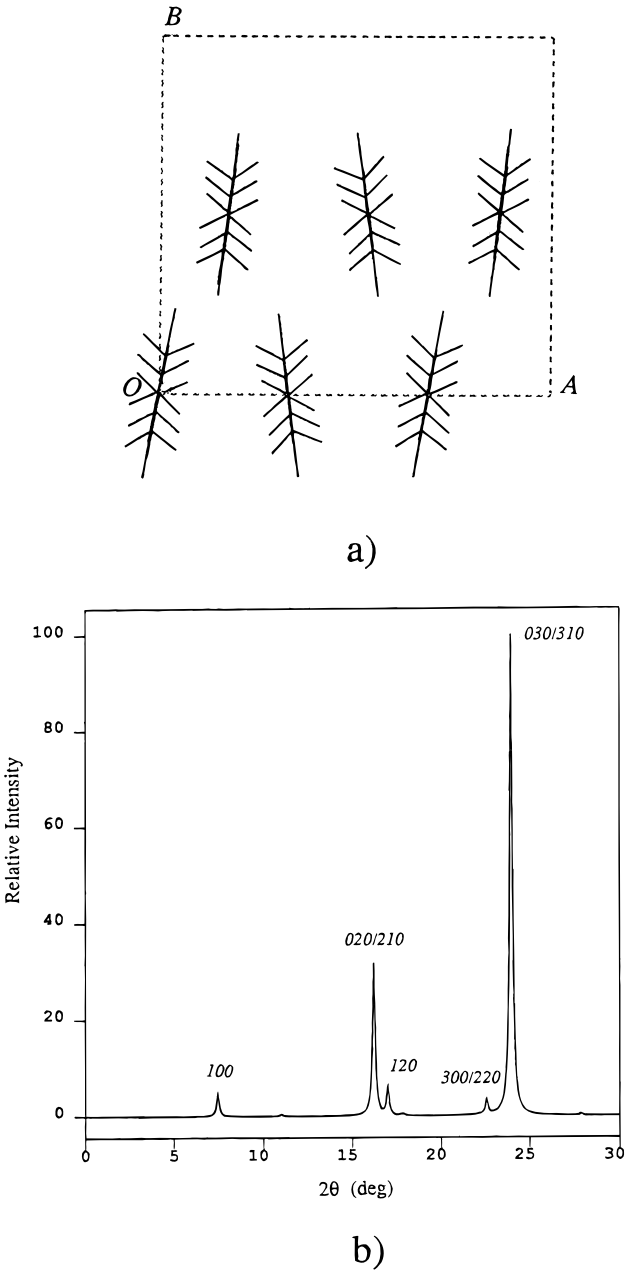

Figure 6. (a) Schematic representation of the chain arrangement projected onto the *ab* plane and (b) calculated intensities of the equatorial reflections of the α-form.

existence of a *c*-glide plane perpendicular to the unique *b*-axis. No systematic absences were observed for reflections of the hkl type. Therefore, the possible space groups are *Pc*, *P*2/*c*, and $P2_1/c$. Various attempts to position the chains led to the choice of the $P2_1/c$ space group. The structure was refined and the calculated structure factors were compared with the experimental values. The lowest *R* index, 14.8%, was obtained for the $P2_1/c$ space group. The calculated fiber pattern is shown in Figure 8a. The final atomic coordinates of the two independent half chains present in the unit cell are given in Table 8. No short van der Waals contacts were detected in this model.

***γ*-form.** The unit-cell dimensions and the molecular packing of the *γ*-form are very reminiscent of those reported for the poly(alkylene terephthalates) (nGT)[29] and the model compound 6BT6. The unit-cell parameters of the *γ*-form and of 6BT6 are very close, except

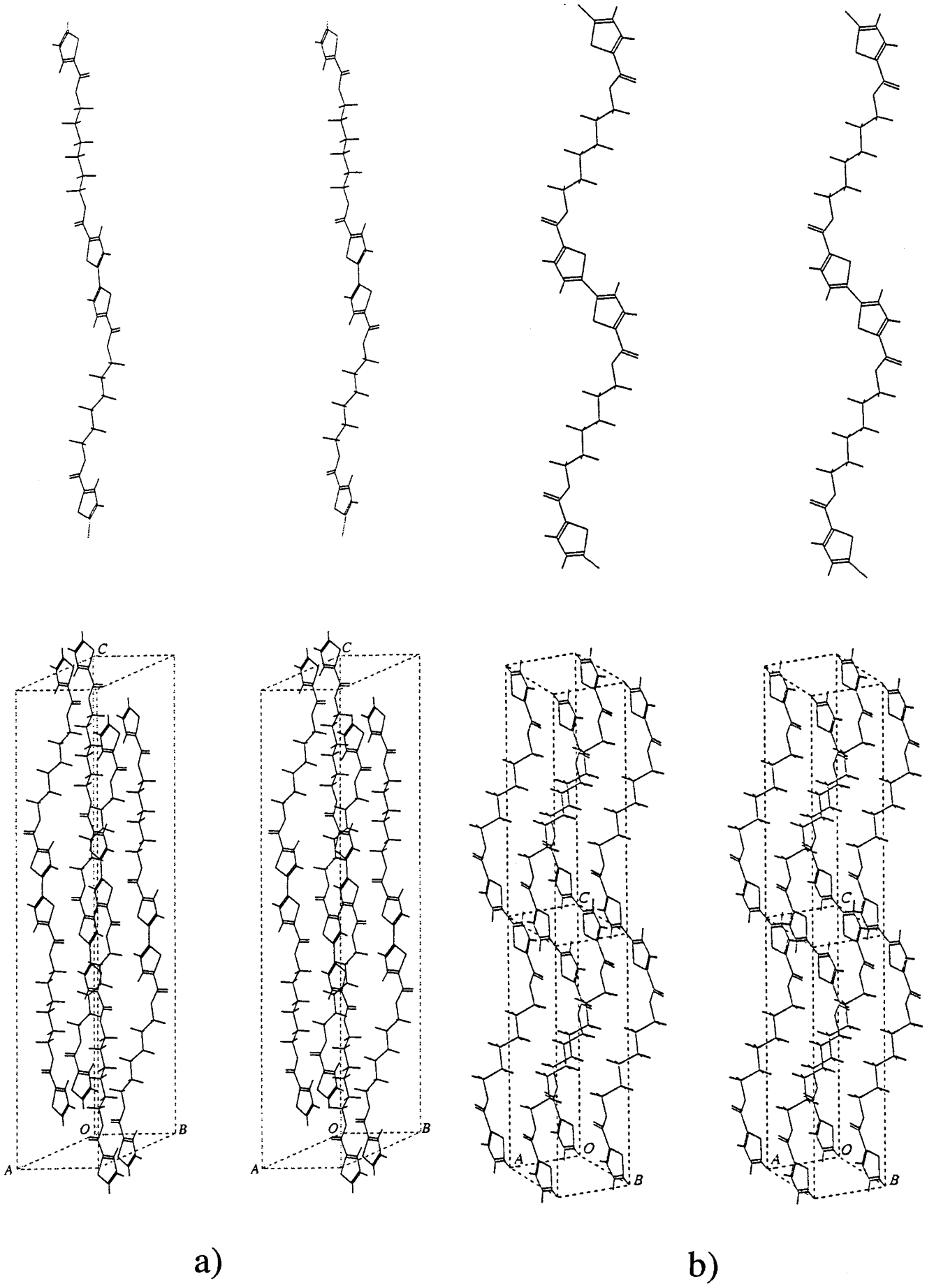

Figure 7. Stereopairs and crystal packing in (a) the β-form and (b) the γ-form.

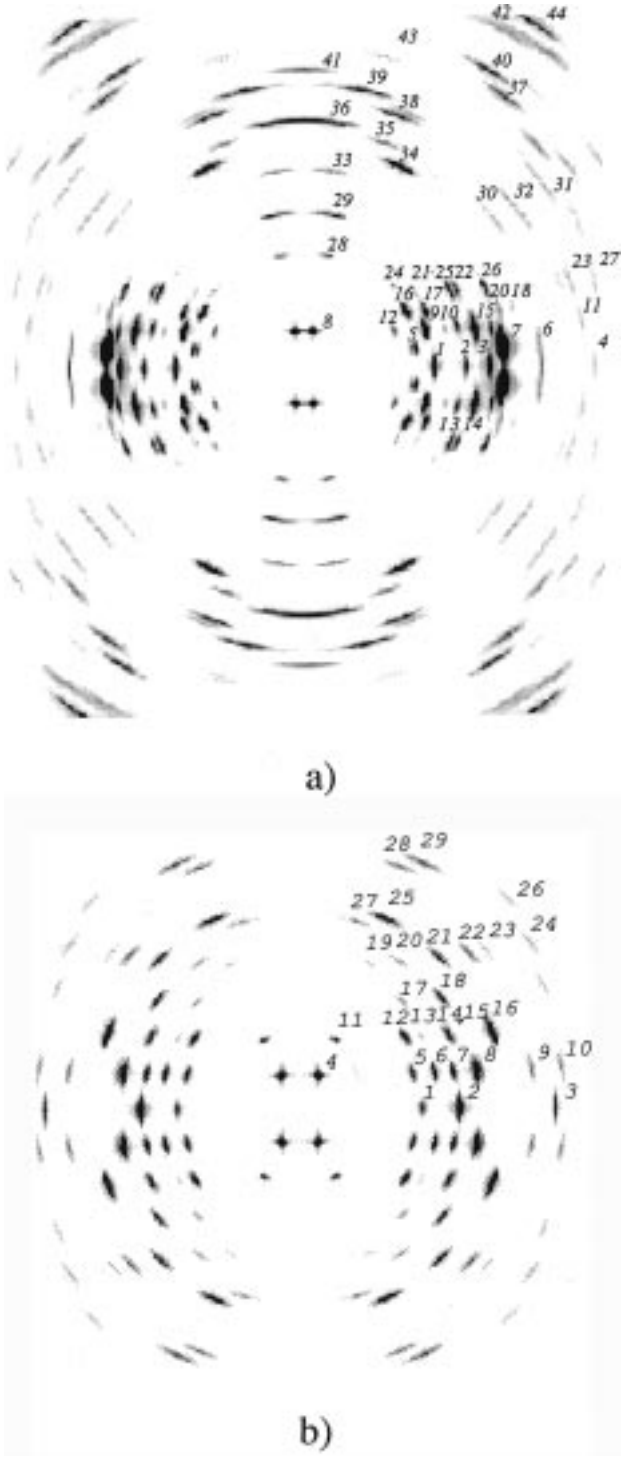

Figure 8. Calculated fiber patterns for (a) the β-form and (b) the γ-form.

for the *c*-axis. As a matter of fact, there is a very strong similarity between the X-ray fiber patterns of the poly(alkylene bithiophenedicarboxylates) with different number of methylenic unit and those of the nGT series. This one-to-one similarity implies that the bithiophene group could be coplanar and behaves like a phenylene plane. Because of this, the chain building and positioning was very much simplified. Energy minimization and structure refinement in the space group $P\bar{1}$ converged to R = 11.6% while the total packing energy reached −39.71kcal/mol. The calculated fiber pattern is shown in Figure 8b. The final atomic coordinates of the γ-form are presented in Table 9. There is only one monomer unit per unit cell. Consequently, the midpoint of the C8−C8′ bond and that of the central bond of the bithiophene group are located on crystallographic centers of symmetry. The crystal packing is characterized by successive layers of aromatic planes and alkylene planes as shown in Figure 7b. The two planar groups, joined by the O2−C6 bond, are twisted around it by 76.8°. The bithiophene moieties are packed in a face-to-face pattern, the interplanar distance is 3.56 Å, a value very close to that found in the 6BT6 model compound, and relatively shorter than 3.7 Å of poly(3-alkylthiophene).[40] The tilt of the bithiophene plane with respect to the *ac* and *bc* planes are 36.9° and 78.3°, respectively. The methylenic sequence is in the *all-trans* conformation. The dihedral angle between the ester O−C═O group and the adjacent thiophene is 1.7°. The carboxylic group is in the trans position relative to the sulfur atom. No inter- or intrachain close contacts are detected.

To follow and confirm the conformational changes taking place in the crystal transformation, the IR spectra for 6BT6 single crystals and polymer fibers in the different crystalline phases were recorded (Figure 9). In the model compound, a strong C═O stretching band was observed at 1725 cm^{-1}, corresponding to the S−C−C═O in the *trans* conformation. In the P6BT fibers, a doublet was found at 1725 and 1700 cm^{-1} due to the isomerization. The higher frequency band is attributed to the *trans* conformation and the lower one can be assigned to the *cis* isomer. Because of the existence of an amorphous phase, these two bands are always observed in the polymer samples. However, the relative intensities are sensitive to the conformational changes in the crystalline phase.[41] In the α- and β-forms, the lower frequency band is always the strongest, confirming that the *cis* isomer is present in both these forms. In the γ-form, the relative intensities are reversed, indicating that the *cis* isomer was transformed into the *trans* isomer.

In addition, based on the combined X-ray structure and IR spectra analyses of tetramethylene glycol dibenzoate derivates,[42] the strong absorbance at 1395 cm^{-1} and the absence of absorption at 1383 cm^{-1} are indicative of the methylenc sequence in an *all-trans* conformation, with torsion angle values near 180°. Meanwhile, in the methylene rocking region, the strong absorption at 950 cm^{-1} and the absence of absorption at 917 cm^{-1} are also good indicators of an *all-trans* methylene confomation.[43]

The Mesophase. One of the interesting phenomena of P6BT is the mesophase behavior. The DSC profiles of Figure 3, show three endothermic peaks corresponding to the phase changes, from the α- to the β- and the γ-form and the melting of the latter. No further peak was observed after melting of the γ-form. On cooling, only one crystallization peak is observed. The DSC curves do not show any significant sign of liquid crystalline behavior. However, when observed under polarized light, a clear birefringent liquid with focal-conic texture was observed after the polymer powder was melted at ca. 172 °C. To avoid the influence of melting of the preformed phase, the same powder sample, whose DSC curve is shown at the top of Figure 3 was employed. Indeed, the powder melted at ca. 173 °C and became a birefringent liquid. The focal-conic texture remains until the temperature exceeds 185 °C. After shearing, no band texture was observed,

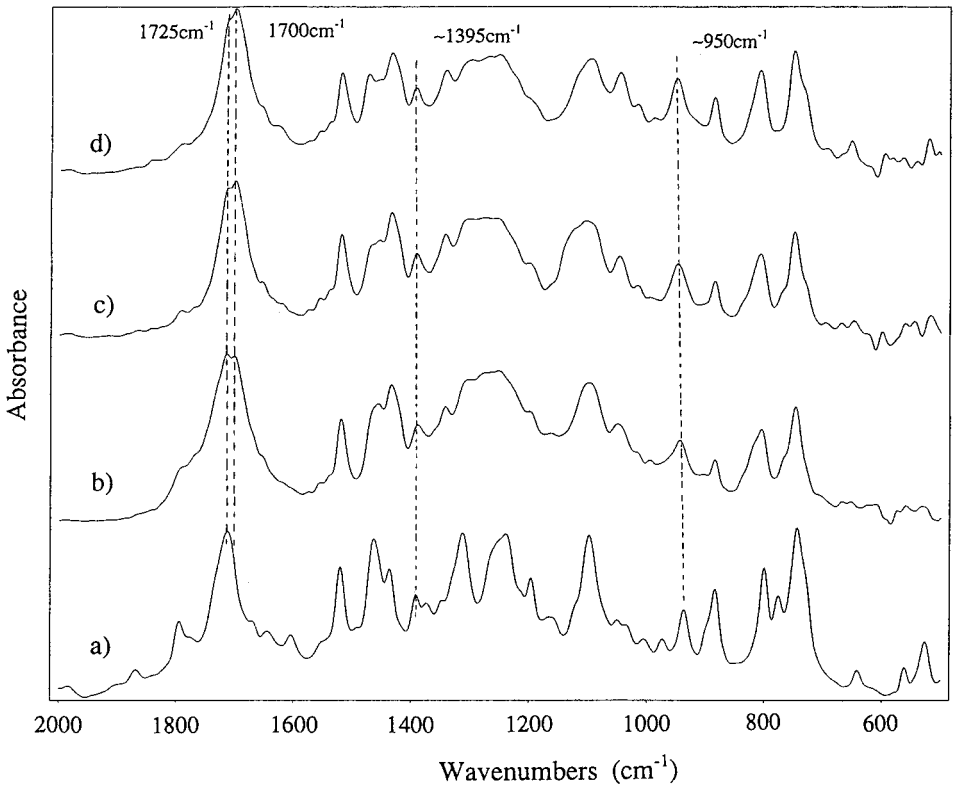

Figure 9. Infrared spectra for (a) 6BT6 single crystals and (b) P6BT fibers of the pure γ-form, (c) the pure α-form, and (d) the β-form (which includes a small fraction of the γ-form).

indicating that the mesophase is probably not nematic. On cooling, the melt crystallized at ca. 145 °C to become a light yellow solid. The focal-conic texture was reproducible in a second heating. A typical texture is shown in Figure 10. To further confirm the liquid crystallinity, the birefringent melt was quenched in liquid nitrogen, and its X-ray powder pattern was recorded. Again, surprisingly, two large angle reflections were recorded, but no small angle reflections characteristic of layer order of a smectic type of mesophase were observed. Obviously, the possibility of smectic packing can be excluded. Then, if one compares the *d*-spacings of these two reflections, 5.42 and 3.77 Å, they are very close to those of the two strongest reflections, (020)/(210) and (030)/(310), of the α-form. This suggests that, in the lateral direction, the molecular chains in the mesophase are arranged in a mode similar to that adopted in the α-form. At the same time, the chains themselves are conformationally disordered and arranged randomly along the chain-axis direction. The chain arrangement is depicted in Figure 11, where a plausible orthogonal packing in the lateral direction, as found in the α-form, was adopted. To our knowledge, this type of mesophase has never been reported. We call it "pseudo smectic-E" simply because of its orthogonal packing and absence of long-range layer order. The occurrence of this unique mesophase may be associated with the strong affinity between aromatic planes in neighboring chains.

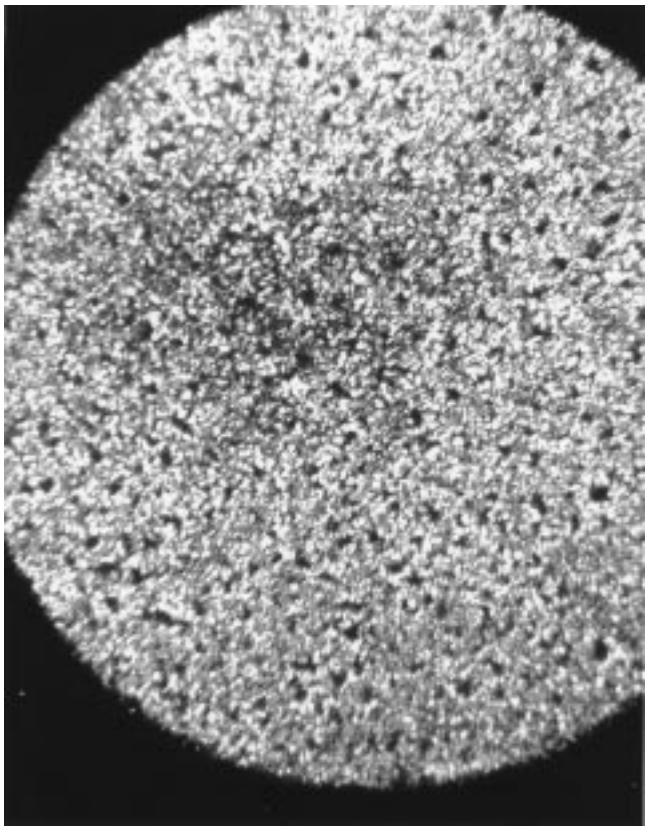

Figure 10. Texture of the P6BT mesophase (×120) recorded at 180 °C.

Conclusions

In this report, the synthesis, crystal structures, and polymorphism of an alternating conjugated and nonconjugated polyester, poly(hexamethylene 2,2′-bithiophene-5,5′-dicarboxylate) (P6BT) were investigated. Three crystalline forms and a monotropic mesophase were identified. The crystal structures were established using the model compound's structural information and chain and packing energy minimization. They are confirmed by a comparison of observed and calculated X-ray structure factors and by an IR conformational

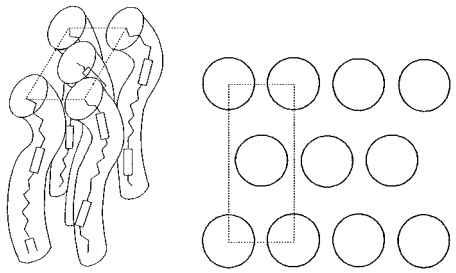

Figure 11. Schematic representation of chain arrangement in "pseudo smetic-E" mesophase: (a) along the chain axis; (b) perpendicular to chain axis.

analysis. Annealing of the raw fiber at low temperature (below 130 °C) yielded the pure α-form. This form is of a paracrystalline nature and may be transformed into the β- and γ- forms by melting and recrystallization mechanisms upon annealing at elevated temperatures. The intermediate β-phase is metastable and can be transformed into the γ-form by a prolonged annealing at a higher temperature. A unique liquid crystalline phase called "pseudo smetic-E" was observed during heating. It is proposed that the chain arrangement in the mesophase bears a very close similarity to the α-form, possessing a two-dimensional orthogonal packing, while the chains themselves are conformationally disordered and displaced randomly along the chain-axis direction.

The crystal structure of a model compound, 6BT6, was determined by single-crystal X-ray diffraction. It was found that the molecule possesses a crystallographic center of symmetry and packs in a triclinic cell. The bithiophenedicarboxylic moiety is confined in the conjugated plane and arranged in a "face-to-face" pattern in the crystal. The methylenic sequence is in a trans conformation, and the whole molecule is of the shape of letter "Z".

The α-form of the polyester belongs to the monoclinic system. There is a translational disorder of the chains along the fiber axis. The chain is in a fully extended conformation, the carbonyl group is in the *cis* orientation relative to the sulfur atom. It is suggested that the structure's characteristics are related to the formation of the mesophase.

The unit cell of the β-form belongs to the monoclinic system, space group $P2_1/c$. The bithiophenedicarboxlic group is planar, and nearly parallel to the *bc* plane. The aliphatic segment is in the *all-trans* conformation. The overall appearance of the chain is that of a sine wave having the a periodicity of 2×19.30 Å.

The fiber pattern of the γ-form reveals the existence of preferred tilt. The tilt angle calculated from film coordinates is 5.2°. The midpoints of the C8−C8′ bond and the C1−C1′ bond coincide with the crystallographic centers of symmetry of the $P\bar{1}$ space group. The bithiophene group is exactly coplanar and the carbonyl group is well confined in the aromatic plane and thus is a well conjugated unit. The carbonyl group is in the *trans* orientation relative to sulfur atom in adjacent ring. The methylenic sequence is in the *trans* conformation. The chain packing is characterized by successive layers where the aromatic planes are arranged in a "face-to-face" pattern, giving rise to π-stacking.

The structures were solved satisfactorily ($R = 14.8\%$ for the β-form and 11.6% for the γ-form) and the conformation was confirmed by IR conformational analysis. In contrast to the common behavior of a shift to shorter wavelengths upon heating, a bathochromic shift was observed. This is attributed to the enhancement of direct interactions between aromatic planes.[43] A detailed study of the related properties such as thermochromism and electrical conductivity observed in this series of alternating conjugated and nonconjugated polyesters will be reported in a forthcoming paper.

Acknowledgment. We thank the National Science and Engineering Council of Canada for its financial contribution.

Supporting Information Available: Tables of structure factors, hydrogen atom coordinates, and anisotropic thermal parameters for 6BT6 (12 pages). Ordering and access information is given on any current masthead page.

References and Notes

(1) Roncali, J. *Chem. Rev.* **1992**, *92*, 711.
(2) Roux, C.; Leclerc, M. *Macromol. Symp.* **1994**, *87*, 1.
(3) Tashiro, K.; Ono, K.; Minagawa, Y.; Kobayashi, M.; Kawai, T.; Yoshino, K. *J. Polym. Sci., Part B: Polym. Phys.* **1991**, *29*, 1223.
(4) Chen, S. A.; Ni, J. M. *Macromolecules* **1992**, *25*, 6081.
(5) Liao, J. H.; Benz, M.; LeGoff, E.; Kanatzidis, M. G. *Adv. Mater.* **1994**, *6*, 135.
(6) Pelletier, M.; Brisse, F.; Cloutier, R.; Leclerc, M. *Acta Crystallogr.* **1995**, *C51*, 1394.
(7) Hong, Y.; Miller, L. L. *Chem. Mater.* **1995**, *7*, 1999.
(8) Kungi, Y.; Miller L. L.; Maki, T.; Canavesi, A. *Chem. Mater.* **1997**, *9*, 1061.
(9) Donat-Bouillud, A.; Mazerolle, L.; Gagnon, P.; Goldenberg, L.; Leclerc, M. To be published.
(10) Li, X.; Brisse, F. *Macromolecules* **1994**, *27*, 7718.
(11) Li, X.; Brisse, F. *Macromolecules* **1994**, *27*, 7725.
(12) Toyoshima, R.; Narita, M.; Akagi, K.; Shirakawa, H. *Synth. Met.* **1995**, *69*, 289.
(13) Watanabe, Y.; Mihara, T.; Koide, N. *Macromolecules* **1997**, *30*, 1857.
(14) Zbinden, R. *Infrared Spectroscopy of High Polymers*; Academic Press: Orlando, FL, 1964.
(15) Gosselin, F.; Di Renzo, M.; Ellis, T. H.; Lubell, W. D. *J. Org. Chem.* **1996**, *61*, 7980.
(16) Sheldrick, G. M. SHELXS96, Beta Test 03 Version. Program for the Solution of Crystal Structures, University of Göttingen, Germany.
(17) Gabe, E. J.; Le Page, Y.; Charland, J. P.; Lee, F. L.; White, P. S. *J. Appl. Crystallogr.* **1989**, *22*, 384.
(18) Sheldrick, G. M. SHELX96, Beta Test 03 Version. Program for the Refinement of Crystal Structures, University of Göttingen, Germany.
(19) *International Tables for Crystallography*; Kluwer Academic Publishers: Dordrecht, The Netherlands, 1992; Vol. C, Tables 4.2.6.8 and 6.1.1.4.
(20) Cambridge Crystallographic Data Centre, 12 Union Road, Cambridge CB2 1EZ, U.K., CSD System Design, Programming and Documentation, October, 1991.
(21) Molecular Simulation Inc., 16 New England Executive Park, Burlington, MA, 01803-5297.
(22) Mayo, S. L.; Olafson, B. D.; Goddard, W. A. *J. Phys. Chem.* **1990**, *94*, 8897.
(23) George, G. Ph.D. Thesis, Université de Montréal, 1997.
(24) Hotta, S.; Waragai, K. J. *Adv. Mater.* **1993**, *5*, 898.
(25) Horowitz, G.; Bachet, B.; Yassar, A.; Lang, P.; Demanze, F.; Fave, J.-L.; Garnier, F. *Chem. Mater.* **1995**, *7*, 1337.
(26) Fichou, D.; Bachet, B.; Demanze, F.; Billy, I.; Horowitz, G.; Garnier, F. *Adv. Mater.* **1996**, *8*, 500.
(27) Pelletier, M.; Brisse, F. *Acta Crystallogr.* **1994**, *C50*, 1942.
(28) Hosemann, R.; Bagchi, S. N. *Direct Analysis of Diffraction by Matter*; North-Holland: Amsterdam, The Netherlands, 1962; Chapter 9, p 302.
(29) Hall, I. H. *Structure of Crystalline Polymer*; Elsevier Applied Science Publishers: Ripple Road, Barking, Essex, England, 1984; Chapter 2, pp 39−79.

(30) Ho, R. M.; Cheng, S. Z. D.; Hsiao, B. S.; Gardner, K. H. *Macromolecules* **1995**, *28*, 1938.
(31) Wang, S.; Wang, J.; Zhang, H.; Wu, Z.; Mo, Z. *Macromol. Chem. Phys.* **1996**, *197*, 4079.
(32) Alemán, C.; Julia, L. *J. Phys. Chem.* **1996**, *100*, 1524.
(33) Ortí, E.; Miruela, P. M.; Sánchez-Marín J.; Tomás, F. *J. Phys. Chem.* **1995**, *99*, 4955.
(34) Visser, G. L.; Heeres, G. J.; Wolters, J.; Vos, A. *Acta Crystallogr. B.* **1968**, *24*, 467.
(35) van Bolhuis, F.; Winberg, H.; Havinga, E. E.; Meijer, E. W.; Staring, E. G. J. *Synth. Met.* **1989**, *30*, 381.
(36) Barbarella, G.; Zambianchi, M.; Bongini, A.; Antonili, L. *Adv. Mater.* **1992**, *4*, 282.
(37) Böhme, O.; Ziegler, C.; Göpel, W. *Synth. Met.* **1994**, *67*, 87.
(38) Destri, S.; Mascherpa, M.; Porzio, W. *Adv. Mater.* **1993**, *5*, 43.
(39) Porzio, W.; Destri, S.; Mascherpa, M.; Brückner, S. *Acta Polym.* **1993**, *44*, 266.
(40) Mårdalen, J.; Samuelsen, E. J.; Gautun, O. R.; Carlsen, P. H. *Synth. Met.* **1992**, *48*, 363.
(41) Koenig, J. L. Spectroscopy of Polymers; ACS Professional Reference Book; American Chemical Society: Washington, DC, 1992; Chapter 3, pp 43−77.
(42) Gillette, P. C.; Dirlikov, S. D.; Koenig, J. L.; Lando, J. B. *Polymer* **1982**, *23*, 1759.
(43) Palmer, A.; Poulin-Dandurand, S.; Brisse, F. *Can. J. Chem.* **1985**, *63*, 3079.

MA9717350